Steffen Schoenhardt, Andreas Boes, Thach G. Nguyen, and Arnan Mitchell
Ridge waveguide couplers with leaky mode resonator-like wavelength responses
Optics Express, 2023; 31(1):626-634

DOI: http://dx.doi.org/10.1364/oe.473131

Research Article Vol. 31, No. 1 / 2 Jan 2023 / Optics Express 626
Optics EXPRESS

Ridge waveguide couplers with leaky mode resonator-like wavelength responses

STEFFEN SCHOENHARDT,[1,2,3] ANDREAS BOES,[1,4,5] THACH G. NGUYEN,[1] AND ARNAN MITCHELL[1,*]

[1]Integrated Photonic Application Center (InPAC), School of Engineering, RMIT University, Melbourne 3000, Australia
[2]Institute of Photonic Chips, University of Shanghai for Science and Technology, Shanghai 200093, China
[3]Center for Artificial Intelligence Nanophotonics (CAIN), School of Optical-Electronic and Computer Engineering, University of Shanghai for Science and Technology, Shanghai 200093, China
[4]Institute for Photonics and Advanced Sensing (IPAS), University of Adelaide, Adelaide, SA 5005, Australia
[5]School of Electrical and Electronic Engineering, University of Adelaide, Adelaide, SA 5005, Australia
*arnan.mitchell@rmit.edu.au

Abstract: Integrated photonic resonators based on bound states in the continuum (BICs) on the silicon-on-insulator (SOI) platform have the potential for novel, mass-manufacturable resonant devices. While the nature of BIC-based ridge resonators requires the resonators to be extended in the (axial) propagation direction of the resonant mode, the requirement for excitation from the quasi-continuum extends the resonator structures also in the lateral dimensions, resulting in large device footprints. To overcome this footprint requirement, we investigate the translation of BIC-based ridge resonators into a guided mode system with finite lateral dimensions. We draw analogies between the resulting waveguide system and the BIC-based resonators and numerically demonstrate that, analog to the BIC-based resonators, such a waveguide system can exhibit spectrally narrow-band inversion of its transmissive behavior.

1. Introduction

Bound states in the continuum (BICs) are unconventional states which are completely lossless and exist amidst a continuum of radiation states. Since the first conceptual description in the context of energy levels of electrons bound to atoms almost 100 years ago [1], BICs have been described in numerous physical systems, for example in electronic, mechanical or photonic systems [2]. The ideal and lossless BIC is completely decoupled from the surrounding radiation states and hence cannot be addressed via the radiation continuum. However, through parameter tuning it is possible to transition from a decoupled BIC into a leaky mode resonator operating near the BIC, which is (weakly) coupled to phase-matched leakage channels and allows exploitation of BIC-like resonances with ultra-high Q-factors. The photonics community has exhibited continuing interest in such high-Q BIC-based resonators [3], which have enabled ultra-high Q-factors exceeding 10^6 in photonic crystal slabs [4]. Furthermore, BIC-based dielectric metasurfaces have shown great potential for applications such as optical beam shaping [5] or spectroscopy in optical biosensing [5].

BICs can also be realized in photonic integrated circuits (PICs), for example in BIC-based waveguiding schemes, which are based on destructive interference of the lateral leakage of leaky waveguide modes [6,7]. When operating the waveguide near a BIC, the waveguide is only weakly coupled to phase matched slab modes, as schematically shown in in Fig. 1(b). The leaky waveguide mode can be engineered through carefully choosing the waveguide width and the etch depth of a silicon on insulator ridge waveguide [8], as schematically shown in Fig. 1(a), or through designing the width and thickness of a low refractive index loading material on a high

#473131 https://doi.org/10.1364/OE.473131
Journal © 2023 Received 12 Aug 2022; revised 21 Oct 2022; accepted 24 Oct 2022; published 23 Dec 2022

Optics EXPRESS

refractive index slab, as demonstrated in [9]. Both cases showed low-loss propagation of the leaky waveguide mode when directly excited.

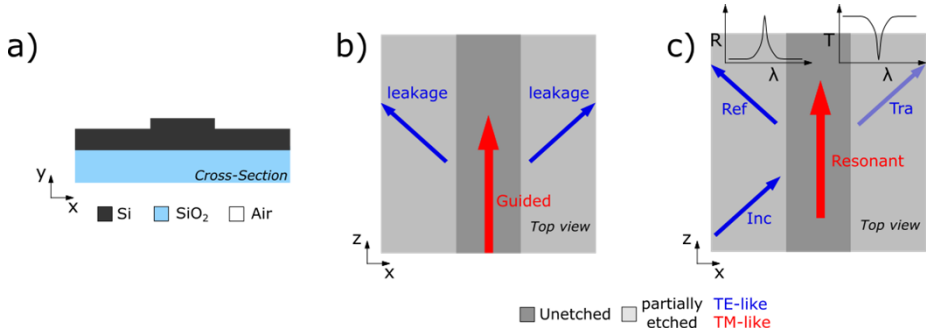

Fig. 1. a) Schematic of a shallow-etched ridge waveguide on the SOI platform, supporting BICs and leaky waveguide modes. b) In BIC-based waveguiding schemes, a leaky waveguide mode near a BIC is excited. At the BIC, destructive interference of the leakage channels allows for low-loss propagation. c) When a waveguide supporting a leaky waveguide mode is excited asymmetrically via a phase-matched leakage channel, it exhibits strong wavelength dependent reflection.

When the leaky waveguide mode is asymmetrically excited through its lateral leakage channel, as schematically shown in Fig. 1(c), spectrally narrow-band reflection of the incident mode can be observed. This behavior has been described for microstrip cavities coupled to slab waveguides [10,11], low refractive index strips on high refractive index slabs [12,13] and for ridge resonators – ridge waveguides with an unbound, partially etched lateral cladding [14], which is the platform that is used as basis for the investigations here. Such BIC-based resonators have been shown to be of particular interest in the context of integrated photonic flat-top filters [15,16].

In our previous experimental demonstration [15], the ridge resonator was excited by a wide Gaussian beam. While our recent work [17] found that the length of the BIC-based ridge resonator is dictated by its target bandwidth and the resonator must extend in the axial propagation direction of the resonant mode accordingly, the lateral dimension of the BIC-based resonant devices was dictated by the space required for shaping the Gaussian excitation beam with on-chip parabolic reflectors. In our previous work, for a resonator with a length of approximately 1 mm, this resulted in a large device footprint of approximately $5{\cdot}10^5$ µm^2[14].

With the motivation to reduce this lateral space requirements for ridge resonators, in this contribution we numerically investigate the excitation of the ridge resonator with wire waveguides. For this purpose, we translate the ridge resonator into a ridge waveguide with finite width of the shallow etched lateral cladding. We conceive a three-waveguide system to asymmetrically excite this ridge waveguide and, analog to the ridge resonator, show this waveguide system to exhibit spectrally narrow-band ($FWHM = 0.5$ nm) inversion of its cross/bar coupling direction with high extinction ration ($ER = 27$ dB).

2. Ridge resonators on a finite slab

The previously presented ridge resonators on an unbound lateral cladding [14] require phase-matching between a (TM-like) leaky waveguide mode and an exciting TE slab mode to exhibit strong reflection. In a ridge on an unbound lateral cladding, the TM-like leaky mode exists among the continuum of TE slab modes. When the unbound cladding is truncated into a finite width, the continuum of TE slab modes will be discretized. In this section, we investigate this translation of the ridge resonator with an infinite width shallow etched lateral cladding to a ridge

Optics EXPRESS

waveguide with finite width of the lateral cladding and analyze the guided modes of the resulting waveguide.

For the investigation, the thicknesses of the waveguiding layers are chosen to be compatible with fabrication parameters in multi project wafer (MPW) foundry fabrication runs [18], which is similar to our previous work [14]. The waveguide is a SOI ridge consisting of a 220 nm thick silicon layer with refractive index $n_{Si} = 3.478$ on a 3 µm thick silica buffer layer with $n_{Oxide} = 1.444$ and air ($n_{air} = 1$) as top cladding. The ridge waveguide is defined by selectively etching the silicon layer to a thickness of 150 nm to form a partially etched lateral cladding and fully etching the silicon layer outside the lateral cladding region to form the lateral boundary of the waveguide as shown in Fig. 2(a). We analyzed the modes of this waveguide structure by using the film mode matching (FMM) method. For a wavelength of 1.55 µm we calculated the modes of a ridge waveguide with a width of $w_{ridge} = 700$ nm as a function of the width of the partially etched lateral cladding (between 2 µm and 5 µm) in increments of 5 nm.

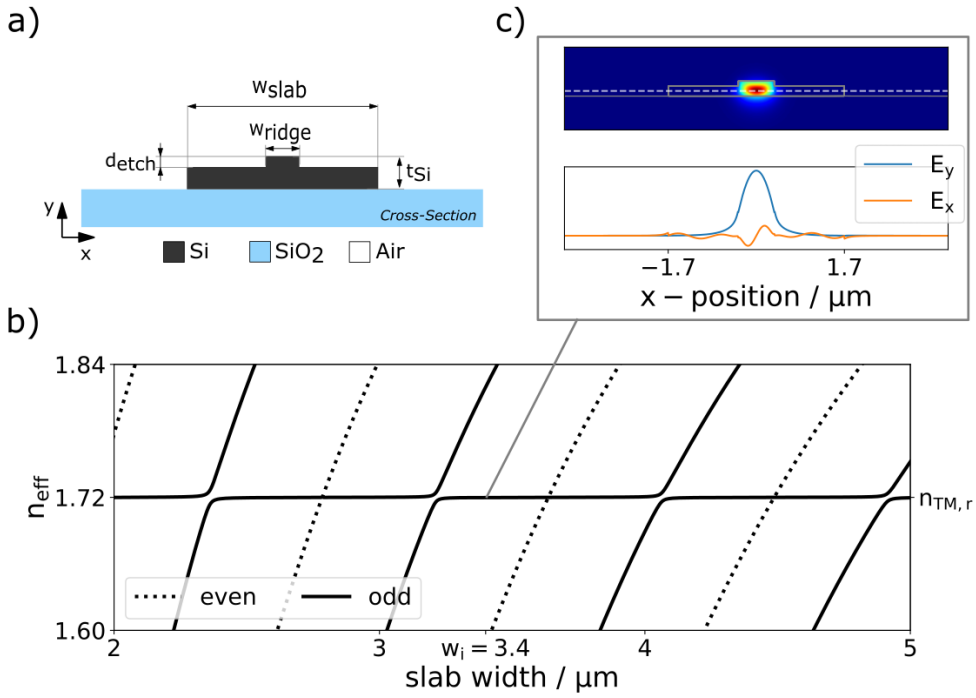

Fig. 2. a) Illustration of the ridge resonator with a lateral shallow etched cladding of finite width. b) Mode effective indices of the waveguide as a function of the width of the partially etched lateral cladding, with modes exhibiting E_x field profiles with even symmetry with respect to the central ridge shown as dotted and odd-symmetric field profiles as solid lines. $n_{TM,r}$ indicates the mode effective index for a ridge waveguide of same dimensions with a laterally unbound partially etched cladding. w_i marks a cladding width at which the ridge mode is spectrally isolated from neighboring cladding modes. c) Top: intensity profile of the TM-like waveguide mode at $w_i = 3.4$ µm, a white dashed horizontal line indicates the position at which the mode profiles shown in the bottom plot are taken. Bottom: Field profiles of the x- and y-oriented electric field components of the ridge mode.

Figure 2(b) shows the recorded mode effective indices as a function of the shallow etched cladding width w_{slab}. Within the effective index range of 1.6 to 1.84, there are two sets of modes: a TM-like mode with effective index almost independent of the slab width, and a discrete set of TE-like cladding modes. For increasing cladding width, the mode effective indices of cladding

Optics EXPRESS

modes increase. When a cladding mode is phase-matched to the ridge mode with effective index $n_{TM,\,r} = 1.72$, it either forms an avoided crossing (for odd-symmetrical cladding modes) or a crossing (for even symmetries) with the ridge mode. The intensity profile of the ridge mode at a cladding width of $w_i = 3.4$ µm (top) as well as the field profiles of the x- and y-oriented electric field components taken at the half-height of the partially etched cladding are shown in Fig. 2(c). While the dominant E_y field component shows an even symmetry with respect to the waveguide center and is confined to the central ridge, the E_x field component shows an odd symmetry and extends throughout the partially etched cladding.

This shows that, analog to the leaky waveguide mode in a laterally unbound ridge waveguide, the TM-like waveguide mode of the ridge waveguide discussed in this section is accompanied by a TE-like field component that extends throughout the partially etched lateral cladding. Due to the symmetry of this TE-component, the ridge mode can hybridize with odd-symmetric cladding modes and become degenerate with even-symmetric cladding modes. This suggests that fields extending through the partially etched cladding, given that they show the right symmetry with respect to the ridge, can couple to the TM-like waveguide mode. Similar behavior was previously observed for tapered ridge waveguide structures in the context of mode polarization converters in PICs [19,20]. In order to couple an external field only to the ridge mode, while avoiding coupling to the cladding modes extending through the slab, careful design of the width of the lateral cladding is required. By choosing a slab width away from crossings or avoided crossings, like the slab width w_i in in Fig. 2(b), we can achieve spectral separation of ridge and cladding modes.

3. Concept of a ridge waveguide coupler

The analogy between the TM-like ridge modes in the laterally unbound ridge resonator and the ridge waveguide system we discussed in the previous section raises the question, whether effects that were observed for ridge resonators can also be observed in such a guided mode system. The key characteristic of the BIC-based ridge resonators is the strong reflection of an incoming beam when asymmetrically excited through a slab mode.

In this section, we introduce wire waveguides symmetrically on either side of the lateral cladding to couple to the ridge waveguide on the finite slab and investigate if such a coupled waveguide system can behave similarly to infinite wide shallow etched cladding system. In the following, we first analyze the modes of this ridge waveguide coupler system before investigating the transmission spectrum of such a ridge waveguide coupler.

3.1. Mode analysis of the ridge waveguide coupler

In Section 2, we found that the TM-like ridge mode can hybridize or become degenerate with modes of the partially etched lateral cladding, depending on the symmetry of the cladding modes. In this section we introduce a pair of wire waveguides symmetrically adjacent to the ridge waveguide, thus adding an additional pair of modes with odd- and even symmetry with respect to the central ridge. The width of the wire waveguide is chosen to $w_{wire} = 325$ nm, so that it supports a quasi-TE mode with an effective refractive index that matches the effective refractive index $n_{TM,\,r}$ of the quasi-TM mode in the central ridge waveguide. The total width of the partially etched lateral cladding is chosen to $w_{slab} = 3.4$ µm, as indicated by the marker w_i in Fig. 2(b). As discussed in the previous section, this width was chosen in order to have the ridge and wire waveguide modes spectrally isolated from the modes supported by the partially etched lateral cladding. The gap between the wire waveguides and the partially etched lateral cladding of the ridge waveguide is chosen to $w_{gap} = 580$ nm, making sure that the wire waveguide modes are only weakly coupled to the cladding of the central ridge.

To investigate the interaction of the modes, we first calculated the waveguide mode effective indices of the odd- and even-symmetric wire waveguide mode pair as well as for the ridge

Optics EXPRESS

waveguide mode as a function of the wavelength, see Fig. 3(b). We also sampled the E_x field profiles of these modes at the half-height of the partially etched ridge waveguide cladding at wavelengths $\lambda = 1.54$ µm, 1.5427 and 1.545 µm (marked i – iii), the field profiles are shown in Fig. 3(c). From the mode field profiles, we can identify the polarization and symmetry of each mode at different wavelengths. Initially (i), the mode effective indices of the odd- and even symmetric wire waveguide modes (black and brown colored lines) evolve approximately parallel with wavelength, showing a mode separation of $\Delta n_{\mathrm{eff,O/E}} = 1.27 \cdot 10^{-4}$. The mode profiles exhibit a strong field in the wire waveguides and weakly oscillating field across the partially etched cladding. The E_x-component of the ridge waveguide mode (light blue line) has an odd symmetry with respect to the central ridge, the field is strongest in the central ridge region and oscillates sinusoidally across the cladding, a small field amplitude can be observed in the wire waveguides.

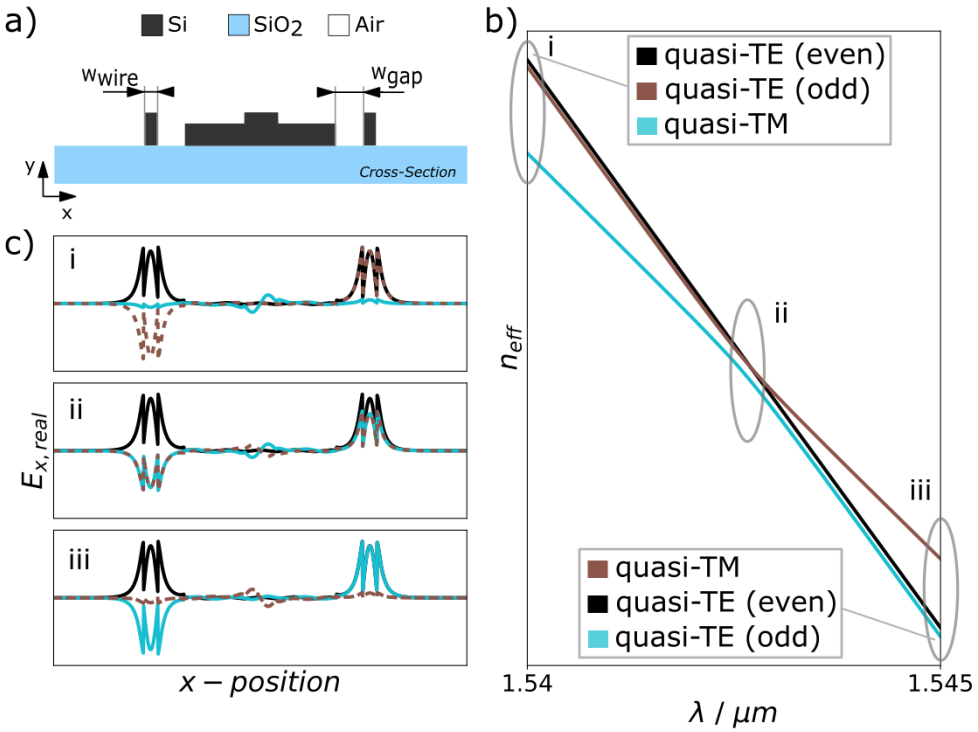

Fig. 3. a) Cross-section of the proposed ridge waveguide coupler. The two wire waveguides on either side of the central ridge waveguide are chosen so that their quasi-TE waveguide modes are phase-matched to the quasi-TM mode of the central ridge. b) Mode effective index of rail and wire waveguide modes as a function of wavelength. (i) The odd- and even symmetric wire waveguide modes are well separated from the quasi-TM ridge mode. (ii) Due to different dispersion characteristics of the wire waveguide and ridge modes, the modes become phase-matched. The even- and (hybridized) odd symmetric wire waveguide modes become degenerate. (iii) The odd-symmetric modes of the waveguide system changed roles, with the former odd-symmetric wire waveguide mode now being the quasi-TM ridge mode and vice versa. c) The mode profiles at the wavelength indicated in b).

For increasing wavelength, the spectral separation between the wire waveguide modes and the ridge mode decreases, until the ridge waveguide mode and the odd-symmetric wire waveguide mode start hybridizing (ii). The field profiles of the hybridized ridge mode and the odd-symmetric wire waveguide mode show comparable amplitudes across the waveguide system but exhibit opposite signs of the field amplitude around the central symmetry plane. We determine the

Optics EXPRESS

minimum difference in effective refractive index between the odd-symmetric wire mode and the ridge mode to be $\Delta n_{\mathrm{eff,O/R}} = 2.5{\cdot}10^{-4}$. For further increasing wavelength the spectral separation between ridge mode (now brown solid line) and wire waveguide mode pair (now black and light blue lines) increases again. The mode effective indices of the odd- and even-symmetric wire waveguide modes again develop approximately parallel with wavelength (iii). The field profile of even-symmetric wire waveguide mode (black solid line) remains unaffected in shape and amplitude by this transition, its mode effective index develops approximately linear with wavelength.

The results shown in Fig. 3 support our hypothesis that the additional wire waveguide modes symmetrically introduced adjacent to the ridge waveguide behave like the quasi-TE modes of the ridge waveguides lateral cladding. When phase-matched, the ridge mode only hybridizes with the odd-symmetric wire waveguide mode while the even-symmetric wire mode remains unaffected. Due to the different dispersion characteristics of wire waveguide and ridge modes, the hybridization of the odd-symmetric modes is restricted to a narrow wavelength range. The hybridization of the modes over wavelength causes the (hybridized) odd- and even-symmetric wire modes to become degenerate.

3.2. Analysis of the transmission spectrum of ridge waveguide coupler

The previously presented ridge resonators and other BIC-based resonant wavelength filters were shown to exhibit strong reflection off the resonator when the excitation mode was phase-matched to the resonator mode, while non-phase-matched excitation would pass through the resonator unaffected. This describes the functionality of a cross/bar coupler, where injected power is transferred to one of two possible outputs depending on the coupler configuration. In this subsection we show that the ridge waveguide coupler discussed in 3.1, analog the ridge resonators, can show cross/bar coupling behavior with spectrally narrow-band inversion of coupling direction when asymmetrically excited. For this purpose, we investigate the spectral response of the coupler system when extended in the z-direction, as depicted in Fig. 4(a). Based on the evolvement of the modes over wavelength shown in the previous subsection, we hypothesize that such a device, when asymmetrically excited through one of the wire waveguides, would behave like a two-waveguide directional coupler when wire and ridge modes are not phase matched. When the wire waveguide modes are, however, phase matched to the ridge mode, we expect a more complex beat pattern between the even- and hybridized odd symmetric wire and ridge modes to emerge. The beat length of the non-phase-matched modes is thereby approximately double of the phase-matched modes, hence for an accordingly chosen device length L, a sharp drop in transmission to the cross port and peak in transmission to the bar port is expected.

We calculated the transmission through the device over wavelength using the eigenmode expansion method. For each wavelength we excited a total of 5 modes (2 wire waveguide modes, the ridge waveguide mode and one adjacent cladding mode with higher/lower refractive index) such that a superposition of the complex mode amplitudes describes an asymmetric excitation with normalized power in one of the wire waveguides at $z = 0$. The power transmitted into the wire waveguides is calculated as T_{cross} and T_{bar}, see Fig. 4(a). The device length L was determined as half a beat length of a directional coupler through the mode splitting of the odd- and even-symmetric wire waveguide modes away from the phase-matching wavelength. We also visualized the power transfer across the device as an intensity map, where the intensity is the magnitude of the Poynting vector for the fields sampled on the x-z-plane across the device at the half-height of the partially etched silicon layer (75 nm).

The calculated transmission spectrum of T_{cross} and T_{bar} is shown in Fig. 4(b). One can see that for wavelength away from the phase-matching wavelength, at wavelengths of $\lambda = 1.54$ (1.545) µm, the device shows a transmission as high as $T_{\mathrm{cross}} > -0.3$ (−0.35) dB into the cross port, the transmission into the bar port is thereby as low as $T_{\mathrm{bar}} < -14$ (−12) dB, respectively. For

Optics EXPRESS

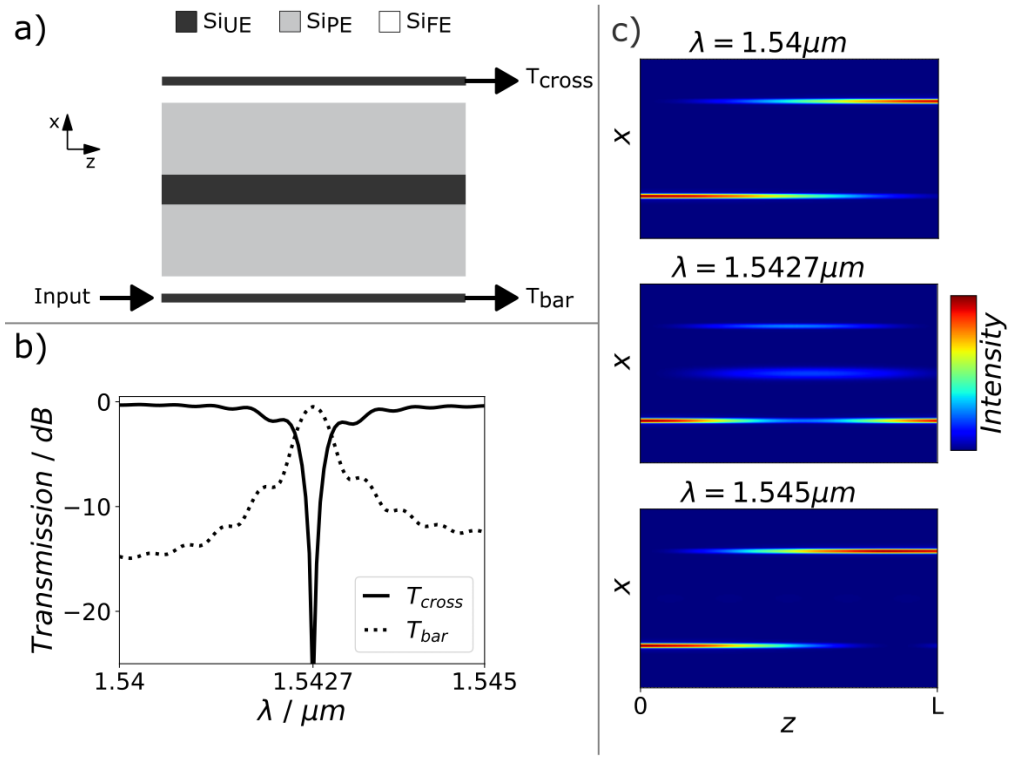

Fig. 4. a) Top view of the proposed ridge waveguide coupler device. The device is asymmetrically excited through the input, the transmission through the device is monitored at the outputs T_{cross} and T_{bar}. Si_{UE}, Si_{PE} and Si_{FE} indicate the unetched (UE), partially- (PE) and fully etched (FE) regions of the waveguide coupler, respectively. b) Transmission spectrum to the cross and bar port of the proposed coupler device c) Intensity sampled at the half height of the unetched slab (110 nm) for a device with $L = 5342$ µm, for a wavelength of 1.54 µm, 1.5427 µm and 1.545 µm.

wavelength approaching the phase-matching wavelength at $\lambda_{\text{PM}} = 1.5427$ µm the transmission pattern of the device is inverted, with the transmission into the cross port de- and the transmission into the bar port increasing. At the phase-matching wavelength, we determine the extinction ratio $ER = T_{\text{cross,max}}/T_{\text{cross, min}} = 27.7$ dB and the 3 dB bandwidth to $FWHM = 0.5$ nm.

Figure 4(c) shows the intensity distribution across the device at and away from the phase-matching wavelength. When the ridge and wire waveguide modes are not phase matched, the intensity distribution shows a pattern that is consistent with a two-waveguide directional coupler configured for cross coupling: Power is injected into the input wire waveguide and transferred into the opposing wire waveguide over the device length. No intensity can be observed in the ridge waveguide in the center of the structure. When the waveguides are phase-matched, on the other hand, a more complex intensity pattern over device length emerges. The intensity map shows again power injected into one wire waveguide at $z = 0$, for increasing device length the intensity distribution evolves to a state where the intensity is distributed across the wire and ridge waveguides, before beating back into a state where most intensity is confined within the input wire waveguide at $z = L$.

The results shown in Fig. 4 describe a three-waveguide coupler device, that shows the typical behavior of a two-waveguide directional coupler but can exhibit a spectrally relatively abrupt change in cross/bar coupling direction. This behavior depends on the phase matching between

Optics EXPRESS

different modes of the system. To compare this device with the original ridge resonator, we determine an analogous Q-factor $Q_{an} = \lambda_{PM}/FWHM = 3085$. We compare this value and the observed *ER* to results published on a ridge resonator of similar dimensions [17], and find that the ridge resonator on a laterally unbound slab shows a higher Q-factor and lower *ER* ($Q \approx 8{\cdot}10^3$, *ER* $\approx$ 6.5 dB). While the results for the Q-factor are in the same order of magnitude, the extinction ratio for the resonator on the open slab is approximately 20 dB lower, less than a quarter of the ER observed here.

In this section we have shown that a three-waveguide directional coupler with a central ridge waveguide supporting a TM-like mode, similar to the ridge resonator on a laterally unbound slab, can exhibit a spectrally sharp inversion of cross/bar coupling direction. Compared to a ridge resonator with the same dimensions of the central ridge, the device discussed in this section shows similar performance in terms of spectral bandwidth better performance in terms of ER. At the same time, with a device width of less than 10 µm, this waveguide coupler has a significantly smaller device footprint in lateral directions compared to the ridge resonator excited via Gaussian beams, which typically requires a device width of several hundred microns. With more than 5 mm, the length of the device is comparable with the length required for the ridge resonator on a laterally unbound slab.

4. Discussion

The ridge waveguide couplers presented in this work are based on phase-matching of modes of different waveguides. As this phase matching depends on the effective indices of the modes involved, the performance of such a device is sensitive to fabrication tolerances. However, the lateral dimensions of the presented device are much smaller than for the ridge resonator devices excited via Gaussian beams. While for a resonator with comparable length, a device based on excitation of the resonator mode via a Gaussian beam would exhibit a footprint of approximately $4{\cdot}10^6$ µm^2, the footprint of the coupler device presented in this work is reduced by almost two orders of magnitude to $5.2{\cdot}10^4$ µm^2. This compact form factor may lead to new ways to investigate BIC-based integrated photonic devices in a scalable way.

This work may be a starting point for a number of investigations into behaviors that have previously been described for BIC-based resonators, and to conceive new platforms or applications of BIC-inspired devices in PICs. For one, while we have previously shown that the spectral response of the ridge resonators in terms of bandwidth and extinction ratio is significantly affected by the length of the resonator [17], we did not investigate this behavior in the present work. We expect that the same behavior is also true for the proposed configuration. Further, the difference in dispersion between the wire waveguide modes and the ridge mode is certainly having an impact on the spectral response of the presented device and could lead to devices with sharper spectral response without affecting the device length. Also, restricting ourselves to a device layout compatible with silicon photonics passive MPW foundry fabrication, we did not consider the possibility of including different materials for wire waveguides, ridge material or material for the partially etched lateral cladding of the ridge that could release some of the limitations we mentioned above, or add functionality such as tunability or switching.

5. Conclusion

In this contribution we have transferred the concept of a ridge resonator on a laterally unbound partially etched slab, into a device with finite lateral dimensions. We have numerically shown that the resulting device, a three-waveguide coupler with a central ridge waveguide supporting a TM-like mode, similar to the ridge resonator, can act as a cross/bar coupler with spectrally narrow-band inversion of its coupling behavior and put this novel device into the context of previously presented ridge resonators. This comparatively compact device may lay the foundation for investigating BIC-inspired integrated photonic components, or other integrated photonic

Optics EXPRESS

components based on the oblique excitation of a structure with 2D cross-section [21], on a scalable platform and could find applications in the fields of optical sensing, on-chip switching and telecommunications.

Funding. Australian Research Council (CE110001018, DP150101336).

Disclosures. The authors declare no conflicts of interest.

Data availability. Data underlying the results presented in this paper are not publicly available at this time but may be obtained from the authors upon reasonable request

References

1. J. von Neumann and E. P. Wigner, "Über merkwürdige diskrete Eigenwerte," in *The Collected Works of Eugene Paul Wigner: Part A: The Scientific Papers*, A. S. Wightman, ed. (Springer, 1993), (pp. 291–293).
2. C. W. Hsu, B. Zhen, A. D. Stone, J. D. Joannopoulos, and M. Soljačić, "Bound states in the continuum," Nat. Rev. Mater. **1**(9), 16048 (2016).
3. S. I. Azzam and A. V. Kildishev, "Photonic Bound States in the Continuum: From Basics to Applications," Adv. Opt. Mater. **9**(1), 2001469 (2021).
4. C. W. Hsu, B. Zhen, J. Lee, S.-L. Chua, S. G. Johnson, J. D. Joannopoulos, and M. Soljačić, "Observation of trapped light within the radiation continuum," Nature **499**(7457), 188–191 (2013).
5. A. Leitis, A. Tittl, M. Liu, B. H. Lee, M. B. Gu, Y. S. Kivshar, and H. Altug, "Angle-multiplexed all-dielectric metasurfaces for broadband molecular fingerprint retrieval," Sci. Adv. **5**(5), eaaw2871 (2019).
6. T. G. Nguyen, A. Boes, and A. Mitchell, "Lateral Leakage in Silicon Photonics: Theory, Applications, and Future Directions," IEEE J. Sel. Top. Quantum Electron. **26**(2), 1–13 (2020).
7. T. G. Nguyen, R. S. Tummidi, T. L. Koch, and A. Mitchell, "Rigorous Modeling of Lateral Leakage Loss in SOI Thin-Ridge Waveguides and Couplers," IEEE Photonics Technol. Lett. **21**(7), 486–488 (2009).
8. M. A. Webster, R. M. Pafchek, A. Mitchell, and T. L. Koch, "Width Dependence of Inherent TM-Mode Lateral Leakage Loss in Silicon-On-Insulator Ridge Waveguides," IEEE Photonics Technol. Lett. **19**(6), 429–431 (2007).
9. Z. Yu, X. Xi, J. Ma, H. K. Tsang, C.-L. Zou, and X. Sun, "Photonic integrated circuits with bound states in the continuum," Optica **6**(10), 1342–1348 (2019).
10. M. Hammer, L. Ebers, and J. Förstner, "Oblique evanescent excitation of a dielectric strip: A model resonator with an open optical cavity of unlimited Q," Opt. Express **27**(7), 9313–9320 (2019).
11. L. Ebers, M. Hammer, M. B. Berkemeier, A. Menzel, and J. Förstner, "Coupled microstrip-cavities under oblique incidence of semi-guided waves: a lossless integrated optical add-drop filter," OSA Continuum **2**(11), 3288–3298 (2019).
12. E. A. Bezus, D. A. Bykov, and L. L. Doskolovich, "Bound states in the continuum and high-Q resonances supported by a dielectric ridge on a slab waveguide," Photonics Res. **6**(11), 1084–1093 (2018).
13. C.-L. Zou, J.-M. Cui, F.-W. Sun, X. Xiong, X.-B. Zou, Z.-F. Han, and G.-C. Guo, "Guiding light through optical bound states in the continuum for ultrahigh-Q microresonators," Laser Photonics Rev. **9**(1), 114–119 (2015).
14. T. G. Nguyen, G. Ren, S. Schoenhardt, M. Knoerzer, A. Boes, and A. Mitchell, "Ridge Resonance in Silicon Photonics Harnessing Bound States in the Continuum," Laser Photonics Rev. **13**(10), 1900035 (2019).
15. L. L. Doskolovich, E. A. Bezus, and D. A. Bykov, "Integrated flat-top reflection filters operating near bound states in the continuum," Photonics Res. **7**(11), 1314–1322 (2019).
16. T. G. Nguyen, K. Yego, G. Ren, A. Boes, and A. Mitchell, "Microwave engineering filter synthesis technique for coupled ridge resonator filters," Opt. Express **27**(23), 34370–34381 (2019).
17. S. Schoenhardt, A. Boes, T. G. Nguyen, and A. Mitchell, "Ridge resonators: impact of excitation beam and resonator losses," Opt. Express **29**(17), 27092–27103 (2021).
18. P. Dumon, W. Bogaerts, R. Baets, J.-M. Fedeli, and L. Fulbert, "Towards foundry approach for silicon photonics: silicon photonics platform ePIXfab," Electron. Lett. **45**(12), 581–582 (2009).
19. D. Dai, Y. Tang, and J. E. Bowers, "Mode conversion in tapered submicron silicon ridge optical waveguides," Opt. Express **20**(12), 13425–13439 (2012).
20. W. D. Sacher, T. Barwicz, B. J. F. Taylor, and J. K. S. Poon, "Polarization rotator-splitters in standard active silicon photonics platforms," Opt. Express **22**(4), 3777–3786 (2014).
21. M. Hammer, L. Ebers, and J. Förstner, "Resonant evanescent excitation of guided waves with high-order optical angular momentum," J. Opt. Soc. Am. B **38**(5), 1717–1728 (2021).